COMSOL
CONFERENCE
2026 SHENZHEN

Simulation of the Frequency Response of a Mach-Zehnder Modulator Actuated by a PZT Chip

Hao Lin[1], Mingjian You[1] and Qiancheng Zhao[1*]
[1]*State Key Laboratory of Quantum Functional Materials, School of Microelectronics, Southern University of Science and Technology, Shenzhen, Guangdong 518000, China*
[*]*zhaoqc@sustech.edu.cn*

Abstract
Despite rapid progress in piezoelectrically actuated integrated photonic devices, a comprehensive multiphysics modeling methodology remains underdeveloped, hindering design optimization and post-fabrication validation. In this work, we present a systematic modeling framework for a tantalum pentoxide (Ta_2O_5) Mach-Zehnder modulator (MZM) actuated by a top-bonded lead zirconate titanate (PZT) chip. A three-dimensional electromechanical finite-element model is established to evaluate the stress distribution in the waveguide layer and to calculate the frequency response of PZT actuation. By leveraging two-dimensional optical mode analysis and the MZM transfer function, the framework can also predict the MZM's static electro-optic tuning efficiency. The simulated tuning efficiency and the 3 dB bandwidth show excellent agreement with our experimental benchmark measurement. This modeling framework provides a systematic approach for optimizing PZT-actuated Ta_2O_5 photonic devices.

Keywords: piezoelectric, stress-optic effect, Mach–Zehnder modulator, frequency response

Introduction

Tantalum pentoxide (Ta_2O_5) has emerged as a promising integrated photonic platform [1] owing to its broad transparency window, low propagation loss, small thermo-optic coefficient [2], high Kerr nonlinearity, and strong stimulated Brillouin scattering response [3]. These compelling merits make the Ta_2O_5 platform highly versatile for a plethora of photonic devices and functionalities, including external laser cavities [2], athermal optical filters [4], supercontinuum sources [3], with one notable exception of active optical modulators. The absence of electro-optic (EO) response makes direct electrical phase control in Ta_2O_5 waveguides challenging. What is worse, the intrinsically weak thermo-optic response of Ta_2O_5 makes thermal tuning inefficient. Consequently, it is a long-standing hurdle to realizing energy-efficient electrical tuning in the Ta_2O_5 platform.

Fortunately, integrating piezoelectric actuators onto photonic integrated circuits has proven to be an effective strategy to enable passive photonic components with active tunability and high-bandwidth modulation capabilities [5]. For example, lead zirconate titanate (PZT) chips have been integrated onto microring resonators to realize tunable external cavity lasers [6], as well as onto Mach-Zehnder interferometers to achieve highly efficient phase modulation [7]. When electrically biased, the PZT actuator induces mechanical deformation, which in turn introduces stress and strain in the underlying optical waveguide, altering its effective mode index via the stress-optic effect. While the modulation efficiency under static driving conditions has been numerically modeled [8] and has been applied to control resonance splitting [9], a systematic modeling of frequency response under alternating-current driving conditions remains unexplored.

In this work, we develop a 3D finite-element simulation model in COMSOL Multiphysics® to analyze the EO modulation bandwidth of a PZT-actuated Ta_2O_5 Mach-Zehnder modulator (MZM). Adopting the structural geometry from our prior experimental demonstration [7], we establish a simplified 3D model comprising a top PZT actuator bonded to a Ta_2O_5 photonic platform [Fig. 1 (a)]. We first perform a *Stationary* study using the Solid Mechanics (solid) and Electrostatics (es) interfaces within the Structural Mechanics and AC/DC modules to numerically analyze the static stress distribution on the photonic chip. Then, the change in the effective index of the TE mode is evaluated, and the Ta_2O_5 MZM electrical tuning rate is simulated as 30.2 pm/V. Finally, we conduct a *frequency domain* study in the Structural Mechanics and AC/DC modules to model the mechanical strain response as a function of the driving frequency. We obtain a 3 dB bandwidth of 2985 Hz for the PZT-

actuated Ta_2O_5 MZM. Both the simulated electrical tuning efficiency and the 3 dB bandwidth show close agreement with our experimental results [7]. This modeling framework provides a robust design methodology for modeling and optimizing integrated Mach-Zehnder modulators and microring resonators that are actuated by top-bonded PZT chips.

Modeling and Results

As illustrated in Fig. 1 (a), a PZT chip (PA2JEW, Thorlabs) sits on top of one arm of the Ta_2O_5 MZM. It is bonded to the photonic chip via a 100 μm-thick epoxy adhesive layer (Master Bond EP31ND). In our model, the PZT chip is represented as a homogeneous block with a dimension of 3 mm × 3 mm × 2 mm. Its piezoelectric response, however, is anisotropic, with the vertical and the horizontal strains governed by the piezoelectric constants d_{33} and d_{31}, respectively. The cross-section of the underlying Ta_2O_5 waveguide is depicted in Fig. 1 (b). The waveguide core dimension is 2.8 μm × 90 nm. Both the top and bottom silicon dioxide (SiO_2) claddings are 5 μm thick. The top surface of the photonic chip is assumed to be flat to simplify the modeling.

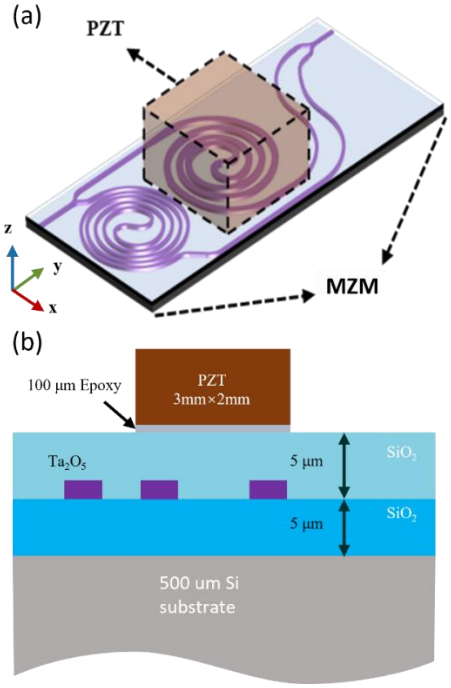


Fig. 1 (a) The 3D artistic illustration of a Ta_2O_5 MZM bonded with a PZT chip on top [7]. (b) The cross-sectional view of the piezoelectric optical modulator.

When an electric field is applied, the converse piezoelectric effect induces deformation in the PZT, which in turn induces mechanical stress in the underlying waveguide layer. The coupling between the strain and the electric field is determined by the constitutive relation [10]:

$$S = s_{\mathrm{E}}T + d^{\mathrm{T}}\vec{E} \quad (1)$$

$$\vec{D} = dT + \epsilon_0\epsilon_{\mathrm{r,T}}\vec{E} \quad (2)$$

where S is the strain, T is the stress, and $\vec{E}$ is the electric field, and $\vec{D}$ is the electric displacement field. The material parameters s_{E}, d, and ϵ_{T}, correspond to the material compliance, the coupling properties, and the permittivity, which are tensors of rank 4, 3, and 2, respectively. The material parameters used in the simulation are listed in Table 1.

Table 1 Material properties employed in the piezoelectric simulation

Parameter	Value	Ref
$d_{33,\mathrm{PZT}}$	2.67×10^{-8} [m/V]	[11]
$d_{31,\mathrm{PZT}}$	-1.20×10^{-8} [m/V]	[11]
$s_{\mathrm{E},11}$	17×10^{-12} [m²/N]	[11]
$s_{\mathrm{E},33}$	23×10^{-12} [m²/N]	[11]
$\varepsilon_{\mathrm{r,PZT}}$	3300	[11]

Stress Distribution

We first perform a *Stationary* study using the Solid Mechanics (*solid*) and Electrostatics (*es*) interfaces within the Structural Mechanics and AC/DC modules to analyze the static stress distribution on the photonic chip. Fig. 2 (a) displays the structural deformation under a DC bias of 10 V. The induced in-plane stresses (S_{x} and S_{y}) along a cut-line is shown in Fig. 2 (b). The cut-line is in the *x*-*y* plane along the *x*-axis. It is in the Ta_2O_5 device layer and passes through the PZT block's vertical central line. These results indicate that the transferred stress is highly spatially dependent, with the central region providing a relatively uniform biaxial stress in contrast to the sharp variations at the edges.

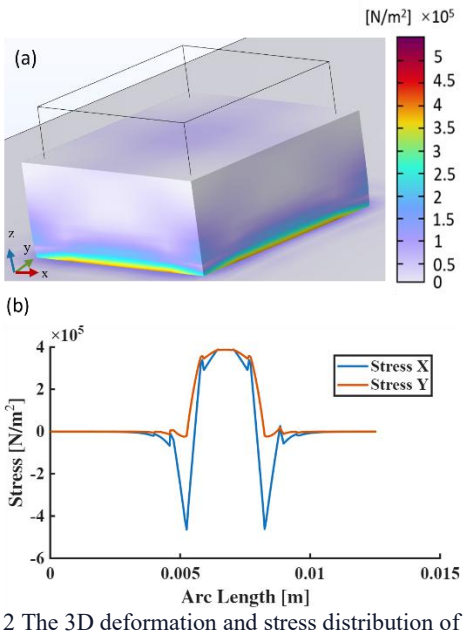


Fig. 2 The 3D deformation and stress distribution of the PZT block bonded to a photonic chip.

Phase Modulation

Utilizing the aforementioned 3D model, the stress components in the waveguide plane are simulated, of which the lateral stresses (σ_x and σ_y) are extracted and fed to another waveguide mode simulator to calculate the waveguide's effective mode index (n_{eff}) [Fig. 3 (a)]. The waveguide mode simulation is realized by the *Mode Analysis* study in the Wave Optics Module. The change in materials' refractive indices caused by mechanical stress can be described by the stress-optic effect:

$$n_x = n_0 - C_1\sigma_x - C_2(\sigma_y + \sigma_z) \quad (3)$$

$$n_y = n_0 - C_1\sigma_y - C_2(\sigma_z + \sigma_x) \quad (4)$$

$$n_z = n_0 - C_1\sigma_z - C_2(\sigma_x + \sigma_y) \quad (5)$$

where n_0 is the material's refractive indices without any stress applied, σ_x, σ_y, and σ_z are the normal stress components, C_1 and C_2 are the first and the second stress optical coefficients. The material properties used in the model are listed in Table 2. The refractive index of the SiO_2 material is assumed stress-independent for simplicity.

Table 2 Material properties employed in stress-optic simulation

Parameter	Value	Ref
n_{0,Ta_2O_5}	2.058	[12]
n_{0,SiO_2}	1.4433	[13]
C_{1,Ta_2O_5}	-2.24×10^{-12} [m²/N]	[9]
C_{2,Ta_2O_5}	1.99×10^{-12} [m²/N]	[9]

The relation between the change of n_{eff} and the applied stress in the *x*-direction (σ_x) as functions of the applied voltage is shown in Fig. 3 (b) The higher the bias voltage, the stronger the stress is, and so is the change of the n_{eff}.

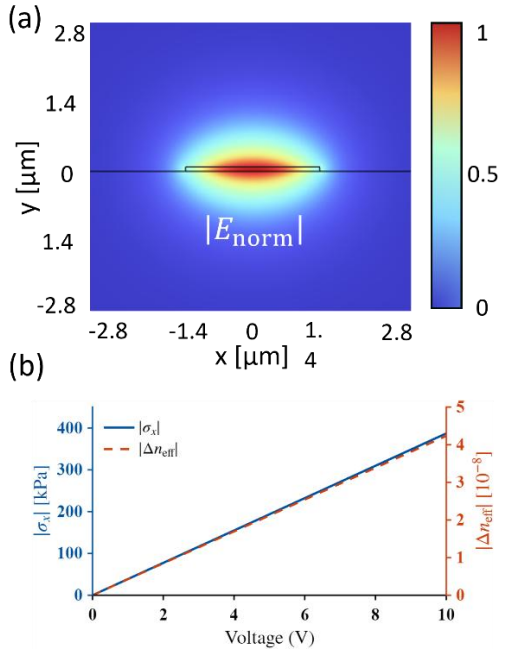


Fig. 3 (a) The normalized waveguide TE_{00} mode profile. (b) The changes of σ_x and n_{eff} versus voltage.

Piezoelectrical Tuning Efficiency

The change of n_{eff} alters the optical phase accumulated in the MZM arm, thereby shifting the MZM's transmission spectrum, which could be theoretically calculated based on the following equation,

$$T = \frac{1}{2}\left\{1 + \cos\left[\frac{2\pi}{\lambda}\left(\left(n_{eff,1}^{(0)} + \Delta n_{eff}\right)L_1 - n_{eff,2}L_2\right)\right]\right\} \quad (6)$$

where L_1 = 31.327 mm is the arm interaction length, L_2 = 31.247 mm is the unmodulated arm length, $n_{eff,1}^{(0)}$ = 1.4773 is the effective mode index of the PZT-actuated arm, $n_{eff,2}$ = 1.4881 is the effective mode index of the unmodulated arm, Δn_{eff} is the effective-index change, and λ is the operating wavelength. Fig. 4 compares the analytical MZM output spectra at 0 V and 10 V. With a 10 V increase in voltage, the resonance minimum is blue-shifted by 302 pm, indicating a tuning efficiency of 30.2 pm/V.

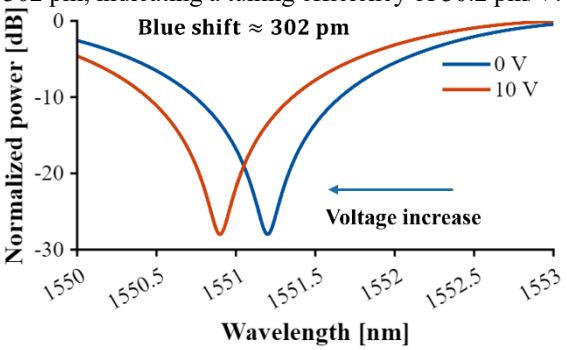


Fig. 4 The analytical MZM output spectra at 0 and 10 V, revealing a resonance blueshift of 302 pm.

Frequency Response

To characterize the frequency response, we then conduct a *frequency domain* study in the Structural Mechanics and AC/DC modules. A frequency sweep from 0 to 5000 Hz is performed at a fixed amplitude of 10 V. By evaluating σ_y at the waveguide layer beneath the PZT center point, the frequency response is obtained in Fig. 5, revealing the 3 dB bandwidth is 2985 Hz. The simulated result aligns well with our experimental measurements [7]. The EO bandwidth is primarily limited to the mechanical damping from the epoxy layer [6].

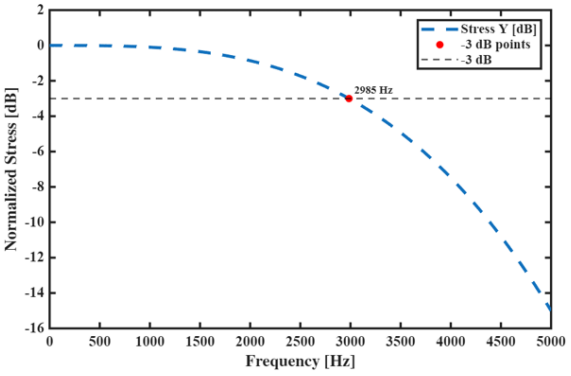


Fig. 5 Frequency Response of y-stress with -3 dB Point

Conclusion

In this work, we develop a 3D modeling framework in COMSOL Multiphysics® to analyze the EO bandwidth and static tuning efficiency of a Ta_2O_5 MZM actuated by a top-bonded PZT chip. By coupling 3D electromechanical stress calculations with 2D optical mode analysis and the analytical MZM transfer function, the framework accurately simulates the voltage-dependent optical transmission spectra and dynamic frequency response. Both the simulated MZM electrical tuning efficiency and the 3 dB EO bandwidth match well with our experimental results. This simulation framework provides a systematic approach for designing and optimizing PZT-actuated integrated photonic devices on Ta_2O_5 platforms, helping elucidate the underlying physics while streamlining device design iterations and improving fabrication yield.

Reference

[1] G. M. Brodnik *et al.*, 'Monolithic 3D integration of tantalum pentoxide nonlinear photonics', *Nature*, vol. 652, no. 8111, pp. 899–905, Apr. 2026, doi: 10.1038/s41586-026-10379-w.

[2] Z. Liu *et al.*, 'Tantalum Pentoxide Integrated Photonics: A Promising Platform for Low-Loss Planar Lightwave Circuits with Low Thermo-Optic Coefficients', *ACS Photonics*, vol. 12, no. 2, pp. 684–695, Feb. 2025, doi: 10.1021/acsphotonics.4c01485.

[3] Z. Liu *et al.*, 'Tantalum Pentoxide Integrated Photonics II: A Promising Photonic Platform for Third-Order Nonlinearities', *ACS Photonics*, vol. 13, no. 8, pp. 2090–2102, Apr. 2026, doi: 10.1021/acsphotonics.5c02597.

[4] M. You *et al.*, 'Athermal Tantalum Pentoxide Mach-Zehnder Interferometers Based on Structural Compensation Method', *IEEE Photonics J.*, vol. 17, no. 1, pp. 1–8, Feb. 2025, doi: 10.1109/JPHOT.2025.3534244.

[5] H. Tian *et al.*, 'Piezoelectric actuation for integrated photonics', *Adv. Opt. Photonics*, vol. 16, no. 4, pp. 749–867, Dec. 2024, doi: 10.1364/AOP.529288.

[6] L. Tang, L. Li, J. Li, and M. Chen, 'Hybrid integrated ultralow-linewidth and fast-chirped laser for FMCW LiDAR', *Opt. Express*, vol. 30, pp. 30420–30429, Aug. 2022, doi: 10.1364/OE.465858.

[7] M. You *et al.*, 'Piezoelectrically tunable athermal Mach-Zehnder interferometer based on a tantalum pentoxide platform', in *Optical Fiber Communication Conference (OFC) 2026*, in Technical Digest Series. Los Angeles, California: Optica Publishing Group, Mar. 2026, p. Tu3C.5. doi: 10.1364/OFC.2026.Tu3C.5.

[8] J. He *et al.*, 'Simulation of Stress-Optic Microresonator Modulator'.

[9] J. He *et al.*, 'Design of Grating-Embedded Tantalum Pentoxide Microring Resonators with Piezoelectric Tunability', *Photonics*, vol. 12, no. 9, p. 903, 2025, doi: 10.3390/photonics12090903.

[10] COMSOL AB, 'Structural Mechanics Module User's Guide', COMSOL Multiphysics v. 5.5. [Online]. Available: https://doc.comsol.com/5.5/doc/com.comsol.help.sme/StructuralMechanicsModuleUsersGuide.pdf

[11] Thorlabs, 'PA2JEW: Piezoelectric Chip with Wires, 75 V, 2.0 µm Travel', Thorlabs, Datasheet CTN003182-S01, Rev. B, Jul. 2020. [Online]. Available: https://media.thorlabs.com/globalassets/items/p/pa/pa2/pa2jew/ctn003182-s01.pdf?v=0116015308

[12] Q. Zhao *et al.*, 'Low-loss low thermo-optic coefficient Ta2O5 on crystal quartz planar optical waveguides', *APL Photonics*, vol. 5, no. 11, p. 116103, Nov. 2020, doi: 10.1063/5.0024743.

[13] M. -S. Kwon, 'Quasi-Phase-Matched Four-Wave Mixing Enabled by Grating-Assisted Coupling in a Hybrid Silicon Waveguide', *IEEE Access*, vol. 10, pp. 83440–83451, 2022, doi: 10.1109/ACCESS.2022.3197286.